A Comparison of Fixed-Parameter Active-Power-Oscillation Damping Solutions for Virtual Synchronous Generators

Yu, Yun; Tinajero, Gibran David Agundis; Chaudhary, Sanjay K; Xu, Luona; Bakar, Nur Najihah Binti Abu; Guerrero, Josep M.; Vasquez, Juan C.

Published in:
IECON 2021 – 47th Annual Conference of the IEEE Industrial Electronics Society

DOI (link to publication from Publisher):
10.1109/IECON48115.2021.9589433

Publication date:
2021

Document Version
Accepted author manuscript, peer reviewed version

A Comparison of Fixed-Parameter Active-Power-Oscillation Damping Solutions for Virtual Synchronous Generators

Yun Yu*, Gibran David Agundis Tinajero, Sanjay K Chaudhary, Luona Xu, Nur Najihah Binti Abu Bakar, Josep M. Guerrero and Juan C. Vasquez
AAU Energy, Aalborg University, Aalborg, Denmark
Email: *yyu@et.aau.dk

***Abstract*—In order to emulate the frequency support characteristics of conventional synchronous generators (SGs), control algorithms based on the virtual synchronous generator (VSG) have been extensively applied to grid-tied converters. However, in the case that a large inertia is used in VSGs, active power oscillations can be introduced in the transients, due to the lack of enough damping effects. To avoid this phenomena, various solutions with additional damping terms have been proposed. This paper analyzes and compares six relevant fixed-parameter active-power-oscillation damping solutions in detail, where responses under set point and phase angle changes, the parameter sensitivity, and capabilities of limiting the rate of change of frequency (RoCoF) and attenuating power ripples are included. The results show the advantages and drawbacks of each solution, leading to the conclusion that extra damping terms may significantly degrade the inertial response of VSGs and have high dependency on the parameter estimation accuracy.**

***Keywords*—Grid-tied converters, virtual synchronous generator (VSG), power oscillation, damping effect.**

I. Introduction

With the rapid development of distributed generation technologies, a large number of power electronic converters have been installed in the grid. Unlike SGs, under transient events, power converters cannot provide inherent inertial response to limit the RoCoF [1], [2]. To solve this problem, the VSG concept has been proposed to emulate the frequency-support characteristics of SGs, where the swing equation is normally used for the design of active power control loops (ACL) [3]–[5]. However, the virtual inertia in VSGs may introduce active power oscillations during transients, which degrades the power quality and increases the risk of overcurrent [6]–[8].

Aiming at providing enough damping effects to attenuate active power oscillations, various fixed-parameter damping solutions have been proposed in the literature. For example, the simplest approach is to increase the damping coefficient in the swing equation, but the static droop characteristic will be changed as well when this coefficient is modified for a better damping performance [9]. Generally, it is not recommended, since an accurate steady-state power sharing largely relies on the droop control [10], [11]. In addition to this solution, extra damping effects can be also embedded by adding the frequency slip that is estimated by the phase-locked loop (PLL) [12], [13]. In this way, additional damping terms for better transients can be realized without affecting the static droop because the frequency slip estimated by the PLL is approximately equal to zero in the steady state. Moreover, by implementing damping correction control through filtering the measured active power, low-frequency oscillations in conventional VSGs can be well attenuated [14]. Although satisfactory damping effects can be attained by applying this solution, degrees of freedom are still not enough to realize any desired damping level and power dynamics. In [15], extra damping terms have been realized through the state-feedback control, where more degrees of freedom are available for adjusting the damping level and power dynamics. Furthermore, in [7], the damping terms were developed based on the relationship between output active power and angular acceleration. The major advantage of using this solution is that degrees of freedom are enough to tune the damping level and power dynamics according to any specific requirement. Additionally, the solution proposed in [8] provides another way to attenuate active power oscillations. However, in this solution, the damping terms could be less effective, since degrees of freedom are less and the tuning of closed-loop poles may be restricted.

For a better understanding of the existing damping solutions, corresponding small-signal models have been derived in section II. The effectiveness of each solution has been analyzed under both nominal and parameter mismatch conditions in section III. Phase angle changes, capabilities in limiting the RoCoF, and capabilities of attenuating power ripples have been evaluated in section III. In section IV, conclusions are given.

II. Modeling of the VSG-Controlled Converter

A. Derivation of Power Equations

The main circuit and control scheme of the studied system is shown in Fig. 1, where the voltage-source converter is connected to the external grid through LC filters. In Fig. 1, R_f and L_f denotes the converter-side resistor and inductor, respectively, and C_f is the capacitor of LC filters. Z_t and Z_g are transformer and grid impedance, respectively, and $Z_L = Z_t + Z_g$ denotes total grid-side impedance.

This work was supported by the Ministry of Foreign Affairs of Denmark, Danida Fellowship Centre (Project No. 19-M03-AAU) and China Scholarship Council (CSC).

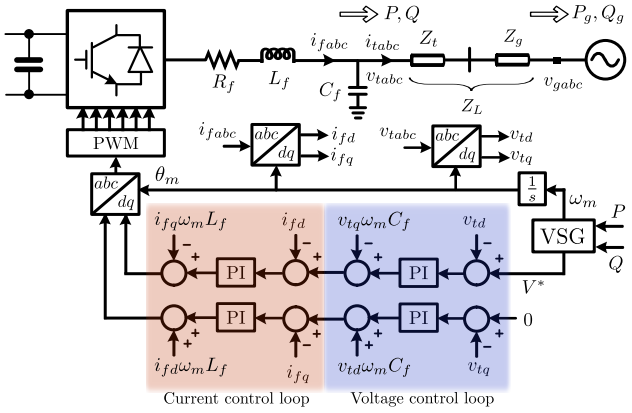

Fig. 1. Simplified diagram of the VSG-controlled converter.

In most applications, both the inner voltage control loop (VCL) and the inner current control loop (CCL) will be applied and designed to ensure a proper regulation accuracy and fast transient responses of converter currents and capacitor voltages. With the bandwidth of VCL and CCL set to the level which is much higher than power control loops, converter currents and capacitor voltages are assumed to be the same as corresponding instantaneous set points. Then, both VCL and CCL can be omitted in the analysis of VSG's dynamics. In this manner, the phasor representation indicated in Fig. 2 can be adopted for the analysis. The diagram in Fig. 2 is given in the signal-phase form, where $\dot{V}_t = V_t \angle \delta$ and $\dot{V}_g = V_g \angle 0$ are used to represent the phasors of capacitor voltages and grid voltages, respectively.

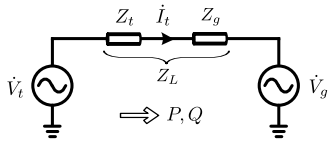

Fig. 2. Phasor representation of the VSG-controlled converter.

In the phasor representation, δ is the power angle which can be written as

$$\delta = \int (\omega_m - \omega_g)\, dt \tag{1}$$

where ω_m and ω_g are angular frequencies of capacitor voltages and grid voltages, respectively.

In this paper, the grid-side network is assumed to be mainly inductive. In the case that the resistance cannot be ignored, virtual impedance loops can be applied to make the equivalent impedance mainly inductive. The total grid-side impedance Z_L can be replaced by the reactance X_L, and the power transferred by the VSG is written as

$$P+jQ = 3\dot{V}_t\bar{\dot{I}}_t = 3\frac{V_T V_g \sin(\delta)}{X_L} + j3\frac{V_T^2 - V_T V_g cos(\delta)}{X_L} \tag{2}$$

Considering a small disturbance near the equilibrium point, linearize (1) and (2), small-signal models of the studied system are derived as follows:

$$\Delta\delta = \frac{1}{s}\left(\Delta\omega_m - \Delta\omega_g\right) \tag{3}$$

$$\Delta P = \frac{\partial P}{\partial \delta}\Delta\delta + \frac{\partial P}{\partial V_T}\Delta V_T + \frac{\partial P}{\partial V_g}\Delta V_g \tag{4}$$

Usually, the variation of grid voltage V_g is assumed to be negligible, and the nominal value of δ is small enough that the coupling effect between active and reactive control loops can be neglected. In this way, (4) is rewritten as

$$\Delta P = \frac{\partial P}{\partial \delta}\Delta\delta \approx 3\frac{V_n^2}{X_L}\Delta\delta \tag{5}$$

where V_n is the nominal phase voltage.

B. Small-Signal Model of the VSG - Case I

The swing equation used for the ACL of conventional VSGs is normally expressed as follows [4]:

$$P^* - P = J\frac{d\omega_m}{dt} + D\left(\omega_m - \omega_0\right) \tag{6}$$

where P^* is the active power set point, P is the output active power, and ω_0 denotes the nominal angular frequency of the grid. J is the moment of the inertia, and D represents the dynamic damping coefficient.

From (3), (5), and (6), the small-signal model which indicates the relationship among the small variations in active power ΔP, the active power set point ΔP^* and the grid phase angel $\Delta\theta_g = \omega_g/s$ can be expressed as

$$\Delta P = \frac{3V_n^2}{JX_L s^2 + DX_L s + 3V_n^2}\Delta P^* - \frac{3V_n^2\left(Js^2 + Ds\right)}{JX_L s^2 + DX_L s + 3V_n^2}\Delta\theta_g \tag{7}$$

From (6), the small-signal model of angular frequency change $\Delta\omega_m$ over the load variation ΔP is derived as

$$\Delta\omega_m = -\frac{1}{Js + D}\Delta P. \tag{8}$$

C. Small-Signal Model of the VSG - Case II

One possibility of increasing the damping effect is to use the addition frequency slip, where the corresponding ACL can be written as follows [13]:

$$P^* - P = J\frac{d\omega_m}{dt} + D\left(\omega_m - \omega_0\right) + D_{pll}\left(\omega_m - \hat{\omega}_g\right) \tag{9}$$

where D_{pll} is the extra damping coefficient corresponds to the additional frequency slip, and $\hat{\omega}_g$ is the estimated angular frequency obtained from the PLL. As it can be observed from (9), the additional damping term is mainly effective during transient processes, since $\omega_m = \hat{\omega}_g$ is approximately achieved in the steady state.

From (3), (5), and (9), the small-signal model in Case II can be derived as

$$\Delta P = \frac{3V_n^2}{JX_L s^2 + \left(D + D_{pll}\right)X_L s + 3V_n^2}\Delta P^* - \frac{3V_n^2\left[Js^2 + \left(D + D_{pll}\right)s\right]}{JX_L s^2 + \left(D + D_{pll}\right)X_L s + 3V_n^2}\Delta\theta_g. \tag{10}$$

For simplicity, impacts of voltage amplitude perturbations on the estimated angular frequency $\hat{\omega}_g$ are neglected. Following this manner, the change in $\hat{\omega}_g$ can be expressed as

$$\Delta\hat{\omega}_g = G_{pll}(s)(\Delta\theta_m - \Delta\theta_{pll})V_n \tag{11}$$

where $\Delta\theta_m = \Delta\omega_m/s$, $\Delta\theta_{pll} = \Delta\hat{\omega}_g/s$, and $G_{pll}(s) = k_{p,pll} + k_{i,pll}/s$. $k_{p,pll}$ and $k_{i,pll}$ are proportional and integral coefficients of the PI regulator used in the PLL, respectively.

From (9) and (11), we have

$$\Delta\omega_m = -\frac{G_{pll}(s)V_n + s}{(Js+D)\left[G_{pll}(s)V_n + s\right] + D_{pll}s}\Delta P. \tag{12}$$

D. Small-Signal Model of the VSG - Case III

Another possibility of implementing additional damping terms is to modify the feedback active power in VSGs, where the ACL can be expressed as follows [14]:

$$P^* - \frac{1+D_f s}{1+T_f s}P = J\frac{d\omega_m}{dt} + D\left(\omega_m - \omega_0\right) \tag{13}$$

where T_f is the low-pass-filter (LPF) coefficient, and D_f is the coefficient for adjusting the additional damping effect.

From (3), (5) and (13), the small-signal model is derived as

$$\begin{aligned}\Delta P = &\frac{3V_n^2\left(T_f s+1\right)}{JX_L T_f s^3 + K_{p2}s^2 + K_{p1}s + 3V_n^2}\Delta P^* \\ &- \frac{3V_n^2\left[JT_f s^3 + \left(J+DT_f\right)s^2 + Ds\right]}{JX_L T_f s^3 + K_{p2}s^2 + K_{p1}s + 3V_n^2}\Delta\theta_g\end{aligned} \tag{14}$$

where

$$K_{p2} = \left(J + DT_f\right)X_L,\ K_{p1} = DX_L + 3V_n^2 D_f. \tag{15}$$

Moreover, from (13), we have

$$\Delta\omega_m = -\frac{1}{Js+D}\frac{1+D_f s}{1+T_f s}\Delta P. \tag{16}$$

E. Small-Signal Model of the VSG - Case IV

By utilizing the state-feedback control, more degrees of freedom can be introduced to tune the power dynamics. The corresponding ACL can be written as follows [15]:

$$\begin{aligned}\omega_m &= \omega_0 + \frac{1}{Js}\left[P^* + P_d - D\left(\omega_m - \omega_0\right) - \frac{1}{1+T_f s}P\right] \\ P_d &= -k_{x\omega}\left(\omega_m - \omega_0\right) - \frac{k_{xp}}{1+T_f s}P - \frac{k_{xi}}{s}P_d\end{aligned} \tag{17}$$

where P_d denotes the virtual damping power, $k_{x\omega}$, k_{xp}, and k_{xi} are feedback and integral coefficients used to generate P_d, and T_f is the LPF coefficient.

From (3), (5) and (17), the small-signal model is written as

$$\begin{aligned}\Delta P = &\frac{3V_n^2\left[T_f s^2 + \left(T_f k_{xi}+1\right)s + k_{xi}\right]}{JX_L T_f s^4 + L_{p3}s^3 + L_{p2}s^2 + L_{p1}s + 3V_n^2 k_{xi}}\Delta P^* \\ &- \frac{3V_n^2\left[JT_f s^4 + L_{z3}s^3 + L_{z2}s^2 + Dk_{xi}s\right]}{JX_L T_f s^4 + L_{p3}s^3 + L_{p2}s^2 + L_{p1}s + 3V_n^2 k_{xi}}\Delta\theta_g\end{aligned} \tag{18}$$

where

$$\begin{aligned}L_{z3} &= \left(Jk_{xi} + k_{x\omega} + D\right)T_f + J, \\ L_{z2} &= Jk_{xi} + k_{x\omega} + D + DT_f k_{xi}, \\ L_{p3} &= L_{z3}X_L,\ L_{p2} = L_{z2}X_L, \\ L_{p1} &= DX_L k_{xi} + 3V_n^2\left(k_{xp}+1\right).\end{aligned} \tag{19}$$

From (17), we have

$$\Delta\omega_m = -\frac{\left(k_{xp}+1\right)s + k_{xi}}{JT_f s^3 + L_{z3}s^2 + L_{z2}s + Dk_{xi}}\Delta P. \tag{20}$$

F. Small-Signal Model of the VSG - Case V

In [7], it was found that active power oscillations can be attenuated by the feedback of angular acceleration and high-frequency components of the active power. The corresponding ACL can be expressed as follows:

$$P^* - \left(\frac{k_{p1}s}{s+k_{p2}} + 1\right)P = \left(J + \frac{k_{\omega1}}{s+k_{\omega2}}\right)\frac{d\omega_m}{dt} + D\left(\omega_m - \omega_0\right) \tag{21}$$

where k_{p1} and k_{p2} are high-pass-filter (HPF) coefficients, and $k_{\omega1}$ and $k_{\omega2}$ are LPF coefficients.

From (3), (5) and (21), the small-signal model is

$$\begin{aligned}\Delta P = &\frac{3V_n^2\left[s^2 + \left(k_{p2}+k_{\omega2}\right)s + k_{p2}k_{\omega2}\right]}{JX_L s^4 + M_{p3}s^3 + M_{p2}s^2 + M_{p1}s + 3V_n^2 k_{p2}k_{\omega2}}\Delta P^* \\ &- \frac{3V_n^2\left[Js^4 + M_{z3}s^3 + M_{z2}s^2 + Dk_{p2}k_{\omega2}s\right]}{JX_L s^4 + M_{p3}s^3 + M_{p2}s^2 + M_{p1}s + 3V_n^2 k_{p2}k_{\omega2}}\Delta\theta_g\end{aligned} \tag{22}$$

where

$$\begin{aligned}M_{z3} &= J\left(k_{p2}+k_{\omega2}\right) + k_{\omega1} + D, \\ M_{z2} &= Jk_{p2}k_{\omega2} + k_{p2}k_{\omega1} + D\left(k_{p2}+k_{\omega2}\right), \\ M_{p3} &= M_{z3}X_L,\ M_{p2} = M_{z2}X_L + 3V_n^2\left(k_{p1}+1\right), \\ M_{p1} &= DX_L k_{p2}k_{\omega2} + 3V_n^2\left(k_{p1}k_{\omega2} + k_{p2} + k_{\omega2}\right).\end{aligned} \tag{23}$$

From (21), we have

$$\Delta\omega_m = -\frac{\left(k_{p1}+1\right)s^2 + \left(k_{p1}k_{\omega2} + k_{\omega2} + k_{p2}\right)s + k_{p2}k_{\omega2}}{Js^3 + M_{z3}s^2 + M_{z2}s + Dk_{p2}k_{\omega2}}\Delta P. \tag{24}$$

G. Small-Signal Model of the VSG - Case VI

In [8], the additional damping term was applied by using HPFs together with VSGs' angular frequency. The corresponding ACL can be formulated as follows:

$$P^* - P = J\frac{d\omega_m}{dt} + D\left(\omega_m - \omega_0\right) + D_v\left(\frac{T_\omega s}{s+T_\omega}\right)\omega_m \tag{25}$$

where T_ω is the HPF coefficient.

From (3), (5) and (25), we have the small-signal model as

$$\begin{aligned}\Delta P = &\frac{3V_n^2\left(s+T_\omega\right)}{JX_L s^3 + N_{p2}s^2 + N_{p1}s + 3V_n^2 T_\omega}\Delta P^* \\ &- \frac{3V_n^2\left[Js^3 + N_{z2}s^2 + DT_\omega s\right]}{JX_L s^3 + N_{p2}s^2 + N_{p1}s + 3V_n^2 T_\omega}\Delta\theta_g\end{aligned} \tag{26}$$

where

$$N_{z2} = JT_\omega + D + D_v T_\omega,\ N_{p2} = N_{z2} X_L,$$
$$N_{p1} = DX_L T_\omega + 3V_n^2. \tag{27}$$

Similarly, from (25), we have

$$\Delta\omega_m = -\frac{s + T_\omega}{Js^2 + N_{z2}s + DT_\omega}\Delta P. \tag{28}$$

III. Assessment of Damping Solutions

In this section, small-signal models derived in Section II have been used for the assessment of different solutions, and all the parameters used in the assessment are given in Table I, where the base value for X_L is V_n^2/S_{base} and the base value for J, D, and D_{pll} is S_{base}/ω_0.

TABLE I
Parameters used in the simulation assessment

Parameters	Values	Parameters	Values
S_{base}	15 MVA	J	12 pu
V_n	$3.3/\sqrt{3}$ kV	D	20 pu
X_L	4.33 pu	ω_0	314 rad/s
D_{pll}	33.33 pu	$k_{p,pll}$	15
$k_{i,pll}$	2	D_f	0.45914
T_f	0.06	$k_{x\omega}$	3.25587×10^6
k_{xp}	5.67873	k_{xi}	10.60307
k_{p1}	13.41540	k_{p2}	29.35938
$k_{\omega 1}$	9.06977×10^5	$k_{\omega 2}$	18.50209
D_v	3.18310×10^6	T_ω	0.15

A. Responses to Set Point Changes

To evaluate dynamic responses of VSGs to set point variations, (7), (10), (14), (18), (22), and (26) are used to generate pole-zero maps indicated in Fig. 3 and step responses shown in Fig. 4. From Fig. 3, it can be observed that, without implementing any additional damping terms, two complex poles of the conventional VSG have a low damping ratio ($\xi = 0.339$). Thus, obvious oscillations at the natural frequency $\omega_n = 2.46$ rad/s can be observed in Fig. 4. However, in the Case II, two poorly-damped complex poles have been moved to well-damped locations ($\xi = 0.903$), and the oscillations observed in conventional VSGs are well attenuated, as shown in Fig. 4. In the Case III, the LPF introduces another close-loop pole. By appropriately choosing the coefficient D_f in the Case III, two complex poles are set to be dominant, and the corresponding damping factor ξ is around 0.9. From Fig. 4, it can be also seen that the additional damping terms in Case III works well to reduce oscillations. Moreover, in the Case IV, the state feedback control introduces two more closed-loop poles, which makes the number of poles increase to four. Among all the four poles, one real pole ($\omega_n = 7.95$, $\xi = 1$) is determined by the LPF coefficient T_f, and the rest three can be independently adjusted. From Fig. 3, it can be seen that another real pole ($\omega_n = 22.2$, $\xi = 1$) is placed far away from two dominant and well-damped complex poles. In the Case V, there are four independently adjustable close-loop poles, and the pole placement is similar to that in Case IV; however, two non-dominant real poles are set far away

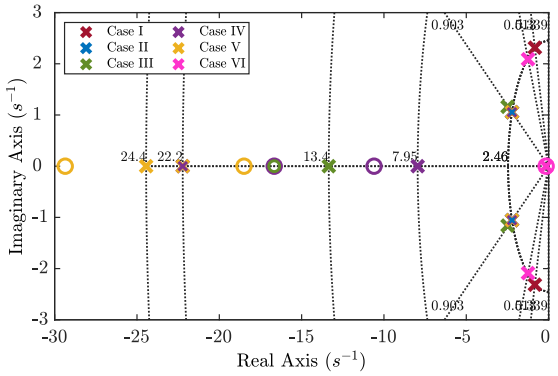

Fig. 3. Poles and zeros of small-signal transfer functions $\Delta P/\Delta P^*$.

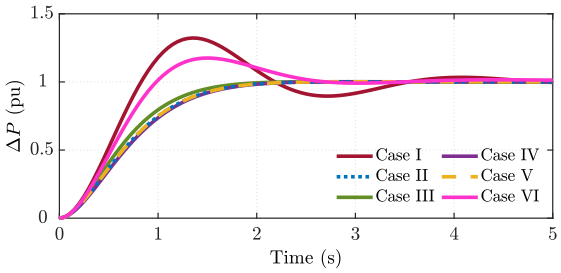

Fig. 4. Responses of VSGs to set point changes $\Delta P/\Delta P^*$.

from two dominant complex poles. In Fig. 4, well-damped responses can be seen in both Case IV and V. Different from aforementioned solutions, Case VI has less degrees of freedom to adjust close-loop poles. Thus, the damping effect in Case VI is weak, and the response in Fig. 4 has oscillations.

B. Parameter Sensitivity

In real applications, the estimation of grid-side reactance X_L is not always accurate. As a result, the effectiveness of applied additional damping terms will be degraded. In order to evaluate impacts of parameter mismatches, the estimated grid-side reactance $\hat{X}_L$ is set to 4.33 pu, while the real grid-side reactance X_L used in (7), (10), (14), (18), (22), and (26) varies from $0.2\hat{X}_L$ to $1.4\hat{X}_L$. As indicated in Fig. 5, in Case I, II and VI, damping ratios of two dominant close-loop poles decrease when the real reactance X_L reduces. Correspondingly, power oscillations start to appear in the transients, as shown in Fig. 6. In Case III, dynamics are dominated by two well-damped complex poles first, and the dominant pole is transferred to one real pole when X_L reduces. Thus, well-damped responses can be always guaranteed, as shown in Fig. 6. Similarly, in Case IV, one real pole moves towards the imaginary axis when X_L reduces; however, two poorly-damped complex poles will get closer to the imaginary axis as well. In general, the responses are well-damped, but oscillations start to be observable in the transients when X_L reduces to $0.2\hat{X}_L$. In Case V, no matter how X_L changes, the dynamics will be determined by two well-damped complex poles, since the rest close-loop poles are far away. In this manner, the damping terms in Case V are always effective, as the results shown in Fig. 6.

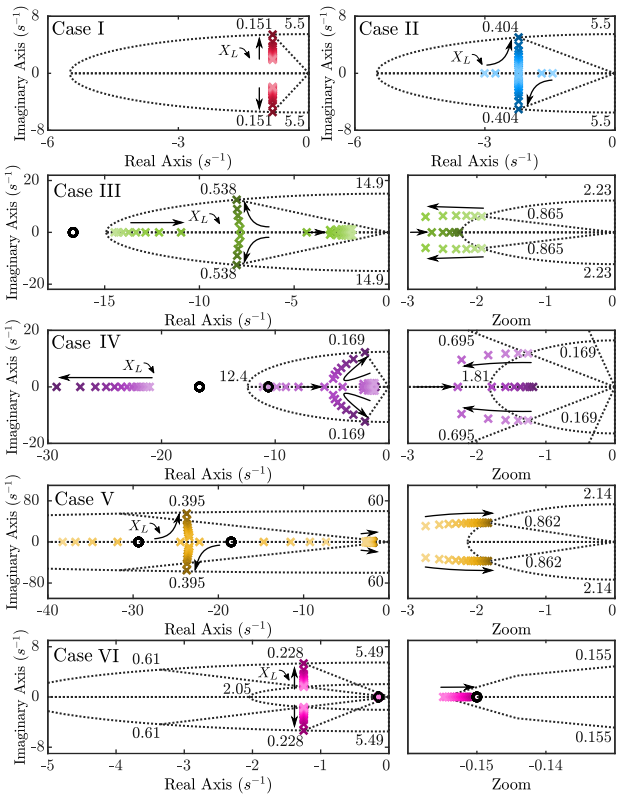

Fig. 5. Poles and zeros of small-signal transfer functions $\Delta P/\Delta P^*$ under grid-side reactance X_L mismatches.

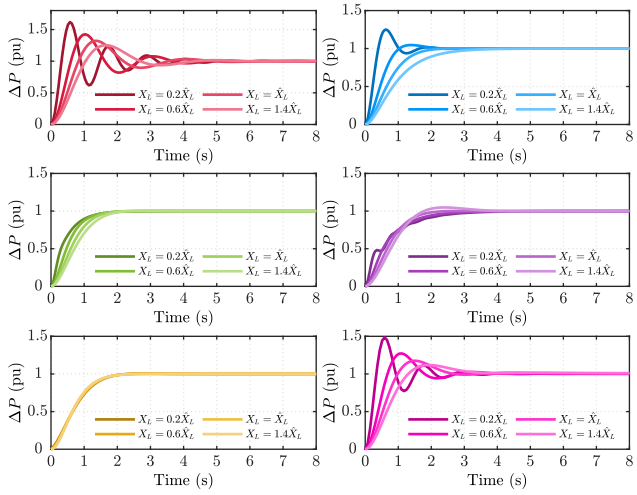

Fig. 6. Responses of VSGs to set point changes $\Delta P/\Delta P^*$ under grid-side reactance X_L mismatches.

C. Responses to Phase Angle Changes

In some cases, the sudden impedance variation inside the grid may cause phase angle changes at terminals of grid-tied converters, which may in turn leads to transients in the power flows, since the power angle δ is inevitably affected. To evaluate the impact of phase angle changes, (7), (10), (14), (18), (22), and (26) are used in the assessment, where the phase

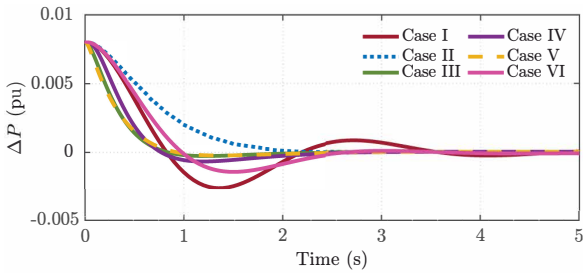

Fig. 7. Responses of VSGs to grid phase angle changes $\Delta P/\Delta\theta_g/S_{base}$.

angle change is set to $1/90$ rad. As shown in Fig. 7, there are still low-frequency power oscillations in Case I and VI. On the other hand, in the rest solutions, dynamics with improved damping performance can be attained, and Case II shows the preferable response where the power perturbation reduces at a slow rate without introducing any negative overshoot.

D. Responses to Load Changes

In order to evaluate that to which extent the virtual inertia helps limit the RoCoF in different solutions, the small-signal transfer function (8), (12), (16), (20), (24), and (28) are used. The corresponding responses of $\Delta\omega_m$ under the unit load change are presented in Fig. 8. The RoCoF in this paper is approximately calculated as follows [9]:

$$\text{RoCoF} = \omega_0\, \Delta\omega_{m,3T}/3T \tag{29}$$

where T is the fundamental period, and $\Delta\omega_{m,3T}$ denotes the value of $\Delta\omega_m$ after three cycles.

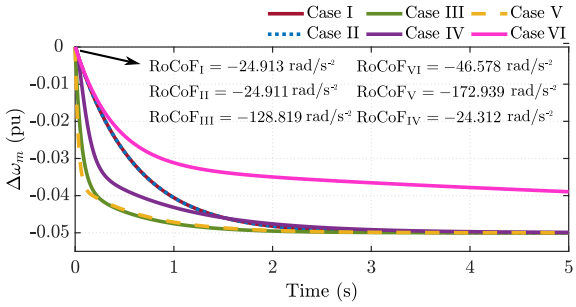

Fig. 8. Responses of VSGs to load changes $\Delta\omega_m/\Delta P \times S_{base}/\omega_0$.

As indicated in Fig. 8, compared with the conventional VSG in Case I, the effect of virtual inertia on limiting the RoCoF is significantly degraded by applying additional damping terms in Case III, IV, and V. Moreover, it also worth noting that the response in Case II is normally worse than the response in real applications where the impact of the PLL can be truly shown. Regarding the response in Case VI, the RoCoF is not degraded; however, the transient process is significantly longer, which extends the time of reaching the predefined steady-state load sharing.

E. Ripple Attenuation Capability

In grid-tied applications, ripples at different frequencies may appear in the measured active power P due to the unbalance

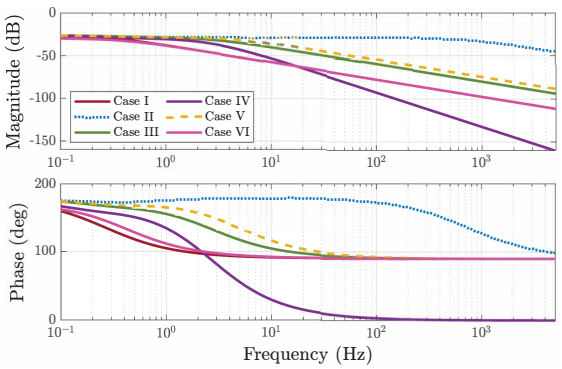

Fig. 9. Frequency responses of $\Delta\omega_m/\Delta P \times S_{base}/\omega_0$.

and harmonics, which in turn has impacts on the control of VSGs. From (8), (12), (16), (20), (24), and (28), the frequency analysis of different solutions is shown in Fig. 9. It can be seen that, when the frequency is above $2\omega_0$, magnitude reduces at the fastest rate in Case IV. Moreover, in Case I and VI, the frequency responses are almost overlapped, and the corresponding ripple attenuation capability is better than that in Case III and V. Among all the solutions, the frequency response in Case II is the worst, since magnitude response is always higher than the rest and varies in a narrow range when the frequency is above $2\omega_0$.

TABLE II
SUMMARY OF THE ASSESSMENT

Case	Power oscillation	Parameter sensitivity	Phase angle response	Limit RoCoF	Attenuate ripples
I	Yes	Sensitive	Inferior	Effective	Average
II	No	Sensitive	Preferable	Affect by PLL	Inferior
III	No	Robust	Average	Degraded	Average
IV	No	Robust	Average	Degraded	Preferable
V	No	Robust	Average	Degraded	Average
VI	Yes	Sensitive	Inferior	Effective	Average

F. Summary of the Assessment

For the benefit of comparison, assessment results are summarized in Table II. Regarding providing damping effects, less effectiveness is shown in Case I and VI; however, in limiting the RoCoF, the most effective results can be attained in Case I and VI. Additionally, in Case III, IV, and V, damping of power oscillations is less dependent on the parameter estimation accuracy. In the case of phase angle changes, the response in Case II is the preferable one among all the solutions. In terms of the ripple attenuation, Case IV shows the best performance, and the response in Case II is the worst.

IV. Conclusion

In this paper, comparative studies have been conducted on fixed-parameter active-power-oscillation damping solutions for the VSG, where response to set point and phase angle changes, the parameter sensitivity, and capabilities of limiting the RoCoF and attenuating power ripples have been included in the comparison. Key findings are listed as follows:

- With more degrees of freedom introduced by the additional damping terms, most solutions can provide same-level damping effects on active-power oscillations when the control coefficients are appropriately tuned.
- In the case of parameter mismatches, the damping effects of some solutions may be significantly degraded. Thus, to propose new damping approaches, parameter sensitivity is an important aspect which needs to be considered.
- In terms of limiting the RoCoF, most solutions evaluated in this paper are not able to provide satisfactory results, which indicates that the additional damping terms have changed the original inertial response of VSGs. Therefore, in order to develop more practical damping strategies, the degradation of inertial responses is an important issue needs to be considered.

References

[1] J. Driesen and K. Visscher, "Virtual synchronous generators," in *Proc. IEEE Power Energy Soc. General Meeting-Convers. Del. Elect. Energy 21st Century*, Jul. 2008, pp. 1–3.

[2] Q. Zhong, "Virtual synchronous machines: A unified interface for grid integration," *IEEE Power Electron. Mag.*, vol. 3, no. 4, pp. 18–27, Dec. 2016.

[3] S. D'Arco, J. A. Suul, and O. B. Fosso, "Small-signal modelling and parametric sensitivity of a virtual synchronous machine," in *2014 Power Systems Computation Conference*, Aug. 2014, pp. 1–9.

[4] S. D'Arco, J. A. Suul, and O. B. Fosso, "Automatic tuning of cascaded controllers for power converters using eigenvalue parametric sensitivities," *IEEE Trans. Ind. Appl.*, vol. 51, no. 2, pp. 1743–1753, Sept. 2015.

[5] Q. Zhong and G. Weiss, "Synchronverters: Inverters that mimic synchronous generators," *IEEE Trans. Ind. Electron.*, vol. 58, no. 4, pp. 1259–1267, Apr. 2011.

[6] W. Du, Q. Fu, and H. F. Wang, "Power system small-signal angular stability affected by virtual synchronous generators," *IEEE Trans. Power Syst.*, vol. 34, no. 4, p. 3209–3219, Jul. 2019.

[7] M. Chen, D. Zhou, and F. Blaabjerg, "Active power oscillation damping based on acceleration control in paralleled virtual synchronous generators system," *IEEE Trans. Power Electron.*, vol. 36, no. 8, pp. 9501–9510, Aug. 2021.

[8] Z. Shuai, W. Huang, Z. J. Shen, A. Luo, and Z. Tian, "Active power oscillation and suppression techniques between two parallel synchronverters during load fluctuations," *IEEE Trans. Power Electron.*, vol. 35, no. 4, pp. 4127–4142, Apr. 2020.

[9] X. Meng, J. Liu, and Z. Liu, "A generalized droop control for grid-supporting inverter based on comparison between traditional droop control and virtual synchronous generator control," *IEEE Trans. Power Electron.*, vol. 34, no. 6, pp. 5416–5438, Sept. 2019.

[10] J. M. Guerrero, J. C. Vasquez, J. Matas, L. G. de Vicuna, and M. Castilla, "Hierarchical control of droop-controlled ac and dc microgrids—a general approach toward standardization," *IEEE Trans. Ind. Electron.*, vol. 58, no. 1, pp. 158–172, Jan. 2011.

[11] J. M. Guerrero, M. Chandorkar, T. Lee, and P. C. Loh, "Advanced control architectures for intelligent microgrids—part I: Decentralized and hierarchical control," *IEEE Trans. Ind. Electron.*, vol. 60, no. 4, pp. 1254–1262, Apr. 2013.

[12] T. Shintai, Y. Miura, and T. Ise, "Oscillation damping of a distributed generator using a virtual synchronous generator," *IEEE Trans. Power Del.*, vol. 29, no. 2, pp. 668–676, Apr. 2014.

[13] J. Liu, Y. Miura, and T. Ise, "A comparative study on damping methods of virtual synchronous generator control," in *2019 21st European Conference on Power Electronics and Applications (EPE '19 ECCE Europe)*, Sept. 2019, pp. 1–10.

[14] S. Dong and Y. C. Chen, "Adjusting synchronverter dynamic response speed via damping correction loop," *IEEE Trans. Power Electron.*, vol. 32, no. 2, pp. 608–619, Jun. 2017.

[15] J. Liu, Y. Miura, and T. Ise, "Fixed-parameter damping methods of virtual synchronous generator control using state feedback," *IEEE Asses*, vol. 7, pp. 99 177–99 190, Jul. 2019.